Numerical Investigation of 3D Effects on a 2D Dominated Flow

Daniel Reese and Chris Weber

Introduction

The interface between gases of two densities will become unstable when accelerated continuously in the direction of the density gradient, resulting in the Rayleigh–Taylor instability [1, 2], or accelerated impulsively in any direction, resulting in the Richtmyer–Meshkov instability (RMI) [3, 4]. These instabilities are governed by the vorticity transport equation,

$$\frac{D\omega}{Dt} = (\omega \cdot \nabla)U - \omega(\nabla \cdot U) + \nu\nabla^2\omega + \frac{1}{\rho^2}(\nabla\rho \times \nabla p), \quad (1)$$

where the non-zero cross product of the density and pressure gradients in the final term will lead to the production of vorticity. The first term on the right of Eq. (1) is the vortex stretching term, where a velocity gradient in the direction of the vorticity vector can lead to an amplification of vorticity and a reduction of its length scale. Eventually this effect can allow the third term on the right of Eq. (1) to dissipate the energy through viscous effects. Vortex stretching is fundamentally a three-dimensional effect and is responsible for the cascade of length scales in turbulent flows [5]. Therefore dissipation and scalar mixing can be expected to increase in three-dimensional flows when compared with two-dimensional flows. Often the RMI and RTI are studied by imposing a well-defined, 2D, single mode perturbation. In experiments, higher mode, 3D perturbations are unavoidable and can eventually grow to break the two-dimensional nature of the interface.

In some regimes, such as inertial confinement fusion and astrophysics, experiments are often modeled in two dimensions due to limited computational resources. In some cases [6], the simulations show clear nonlinearity, therefore it is important to know at what point the 2D simulations diverge from 3D reality. Some ICF experiments [7] are initialized with 2D perturbations for simplicity, but at what point do 3D effects dominate?

The shock tube experiments of Motl et al. [8] used a nominally two-dimensional perturbation to study the Richtmyer–Meshkov instability, but observed turbulent-like features at high Atwood and Mach numbers. We choose this work as the basis for exploring the effects of three-dimensional features. The problem setup and a description of the code used for this study is given in section "Simulation Details". Section "Results" describes the differences in interface growth and mixing due to small-scale and 3D effects. Finally, concluding remarks are given in section "Conclusions".

Simulation Details

The single mode interface used here is based off experimental work [8] which set up a helium-over-SF6 interface (Atwood number = 0.95) with an $\eta = 2.72$ cm amplitude and $\lambda = 16.7$ cm wavelength perturbation. The experiments used several shock strengths, the strongest of which, Mach 1.95, is used here. To compare with the pure single mode case, three-dimensional effects are induced by adding small-scale perturbations. These perturbations were initialized computationally using a Gaussian band in wavenumber space described by

$$A_{RMS}e^{\frac{-(k-k_{peak})^2}{2\sigma^2}} \quad (2)$$

where $k_{peak} = 8\frac{1}{cm}$, $\sigma = 4\frac{1}{cm}$, and $\frac{A_{RMS}}{\eta} = 0.03$. This initial condition is shown in Fig. 1, which shows (a) the single
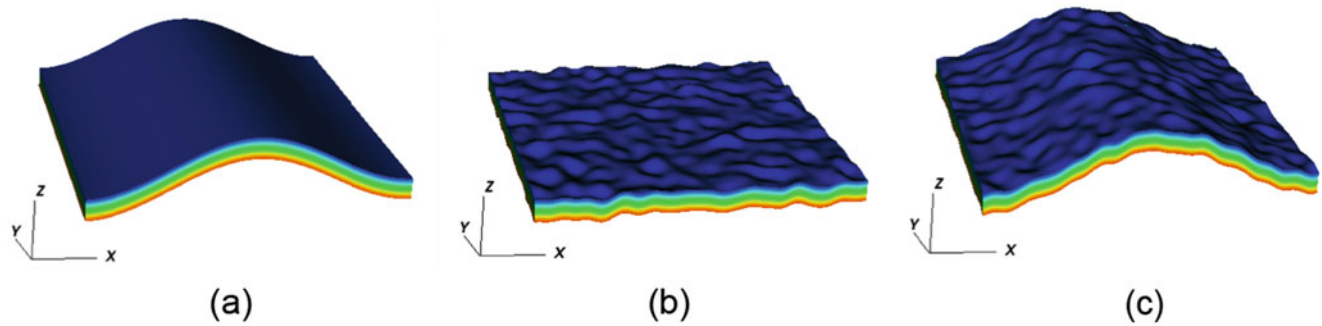
D. Reese (✉)
University of Wisconsin, Madison, WI 53706, USA

Lawrence Livermore National Laboratory, Livermore, CA 94550, USA
e-mail: dtreese@wisc.edu

C. Weber
Lawrence Livermore National Laboratory, Livermore, CA 94550, USA

Fig. 1 Initial condition creation. (**a**) single mode interface (**b**) small-scale perturbations (**c**) initial condition given by the superposition of (**a**) and (**b**)

Table 1 Properties of each simulation

Case	Description	Mesh-size [x($\times$y) z]	Pert. [k_{peak}, σ, $\frac{A_{rms}}{\eta}$]	Single-mode pert. [λ, η, δ]
A	Single mode	256$\times$512	N/A	16.7 cm, 2.72 cm, 0.5143 cm
B	2D	256$\times$512	$8\frac{1}{cm}$, $4\frac{1}{cm}$, 0.03	16.7 cm, 2.72 cm, 0.5143 cm
C	Thin	256$\times$64$\times$512	$8\frac{1}{cm}$, $4\frac{1}{cm}$, 0.03	16.7 cm, 2.72 cm, 0.5143 cm
D	Square	256$\times$256$\times$512	$8\frac{1}{cm}$, $4\frac{1}{cm}$, 0.03	16.7 cm, 2.72 cm, 0.5143 cm
E	High Res.	512$\times$512$\times$1024	$8\frac{1}{cm}$, $4\frac{1}{cm}$, 0.03	16.7 cm, 2.72 cm, 0.5143 cm
F	Small A_{RMS}	512$\times$512$\times$1024	$8\frac{1}{cm}$, $4\frac{1}{cm}$, 0.003	16.7 cm, 2.72 cm, 0.5143 cm

mode perturbation, (b) the small scale perturbations, and (c) the final interface. The cases studied are detailed in Table 1. Two 3D simulations at different resolutions were run to test for convergence, and a 3D simulation with a smaller depth (y-direction) was run to show that a thin domain can be used to capture the 3D effects but save on resources. Finally, a case that used an A_{RMS} value $\frac{1}{10}$ that of the cases mentioned above was also included.

These simulations used the *Miranda* code, a high-order hydrodynamics code developed at Lawrence Livermore National Lab [9]. This large eddy simulation code achieves high spatial accuracy using a 10th-order compact differencing scheme, and is able to achieve high temporal accuracy by using a 4th-order accurate Runge-Kutta scheme. Energy is transported to sub-grid scales through the use of artificial-fluid properties, such as hyper-viscosity and hyper-diffusivity. *Miranda* has proven useful in simulating a large variety of turbulent flows and mixing, including previous RTI and RMI studies [10, 11].

Results

Structure

Figure 2a–d shows slices of volume fraction from several cases in Table 1 at $t = 0$, 0.67, and 1.3 ms after shock acceleration of the interface. This mimics what is seen experimentally using Mie scattering, shown in Fig. 2e. In these images the dense SF_6 is black, the light He is white, and the shock direction was downward. All of these cases show the characteristic behavior of high Atwood number interface growth, where the dense upward going spike becomes very narrow and the downward traveling bubble becomes very broad.

The evolution of the 2D single mode interface, with no small-scale perturbations is shown in (a). When small-scale perturbations are added in 2D, as shown in (b), there is a clear break in the symmetry of the spike structure, and long, drawn-out, black and white filament structures are observed. When the domain is three-dimensional with a depth equal to that of the width, shown in (c), the filament structures have broken into finer scale features and more mixing has occurred, as evident by the presence of more grey area. Similar results are found for a 3D domain with a depth $\frac{1}{4}$ that of the width (not shown). This shows that 3D effects can be captured in a 2D dominated flow with only a narrow 3rd direction. We also found that a twofold increase in resolution for the square 3D computational domain will give little visual difference with the case shown in (c), indicating that results are converged at this resolution. Finally, a case with small-scale perturbations with $\frac{1}{10}$ the RMS amplitude of the previous cases, shown in (d), is included and appears to better match experimental images shown in (e).

Fig. 2 Structure evolution shown at $t = 0$, $t = 0.67$, and $t = 1.3$ ms for (**a**) single mode only (**b**) 2D single mode with perturbations (**c**) square 3D single mode with perturbations (**d**) square 3D with $\frac{1}{10}$ RMS amplitude perturbations (**e**) experiment
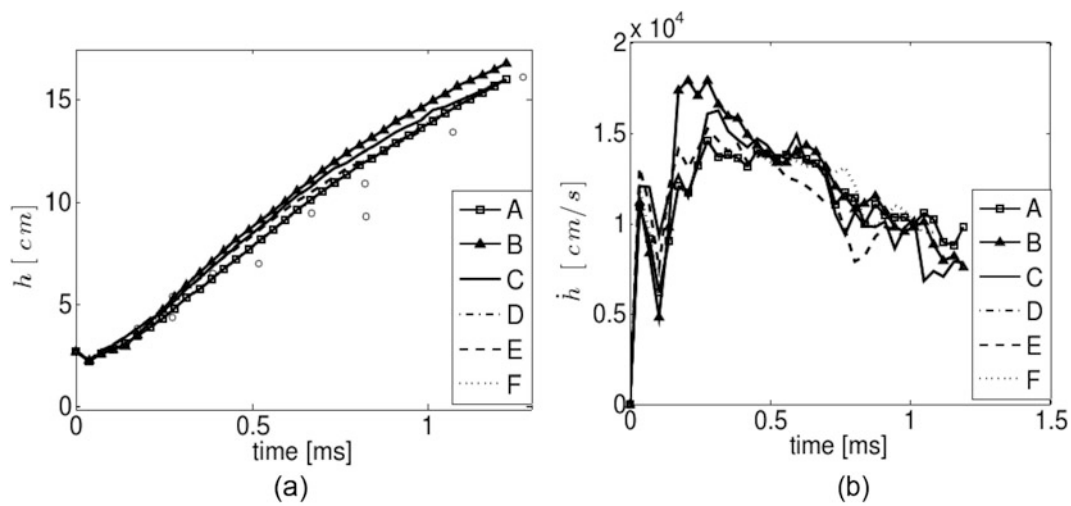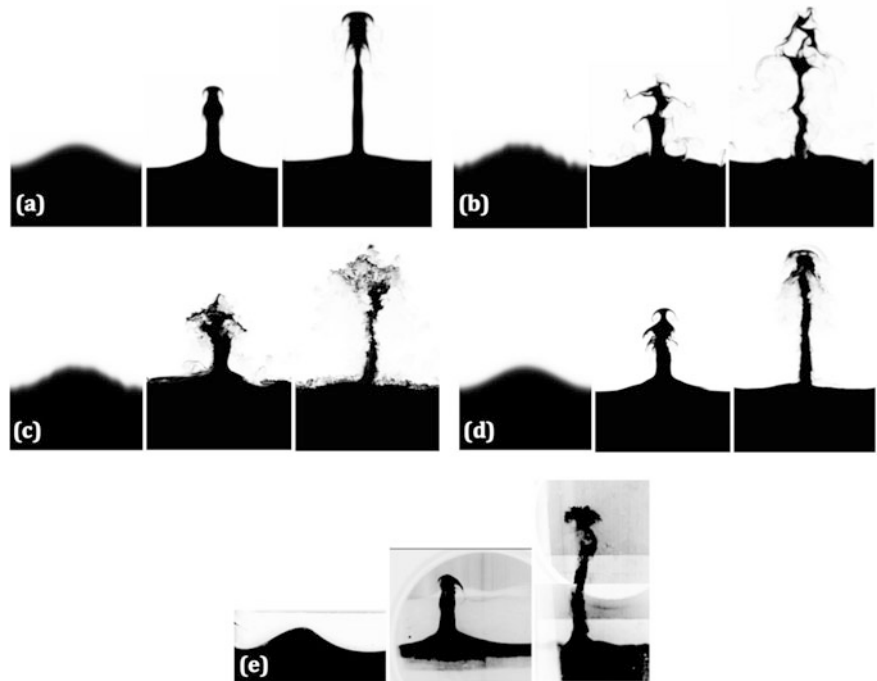

Fig. 3 Spike growth measurements in time. (**a**) height (**b**) growth rate. A: SM; B: 2D; C: 3D Thin; D: 3D Square; E: High Res.; F: Small A_{RMS}. *Open circles* in (**a**) are experimental values

Interface Growth

While small-scale perturbations and three-dimensional effects visually change the interface, their effect on the interface height is small. Here the 50 % contour is used to find the spike-to-bubble height and is compared to the experiments in Fig. 3a. For the 3D cases, 64 slices were used at various depths to find an average height value, modeling the data that might be obtained experimentally through an ensemble average. Figure 3a shows that perturbations increase the growth rate at early time, while 3D effects work to lessen the thickness at late times. This implies that the 2D case may slightly overestimate spike height, but the difference seen here is small. Previous work [12] found 2D simulations to over-predict the experimental interface height, which also seems to be occurring here in 2D and 3D. Growth rates show (Fig. 3b) that there is a small increase in growth from adding small-scale perturbations in 2D and in 3D, but this reduces to a negligible difference in the small A_{RMS} case.
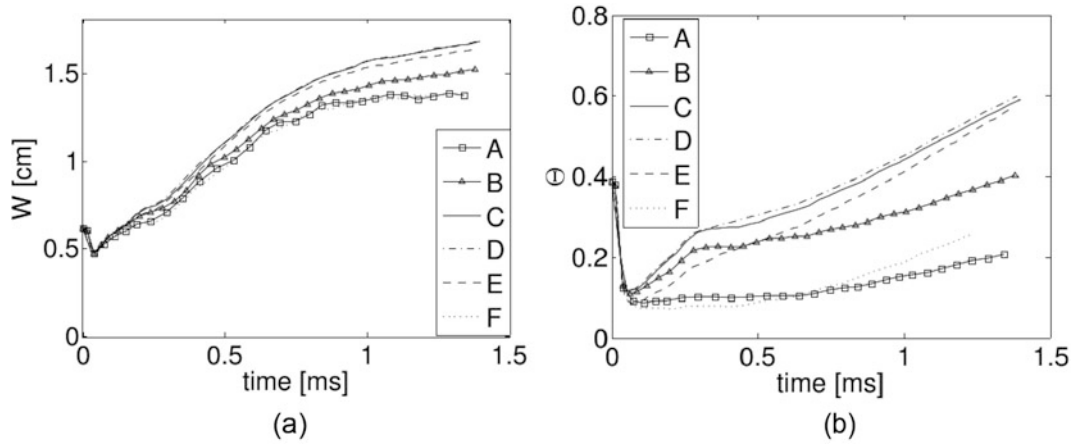
Fig. 4 (**a**) Mixing width in time (**b**) Mixedness in time. A: SM; B: 2D; C: 3D Thin; D: 3D Square; E: High Res.; F: Small A_{RMS}

Mixing

A more detailed description of the structure of the interface is provided by the mixing width and mixing fraction metrics. The integral mixing width is described by

$$W = \int_{-\infty}^{\infty} \overline{\xi}(1 - \overline{\xi}) \, dz \qquad (3)$$

where ξ is the volume fraction and the average volume fraction is given by

$$\overline{\xi} = \frac{1}{L_x} \int_{0}^{L_x} \xi \, dx. \qquad (4)$$

The development of the mixing width is shown in Fig. 4a. There is a slight difference between each case, with a larger mixing width occurring for initial conditions containing small-scale perturbations (B–E). Furthermore, the 3D mesh containing small-scale perturbations (C–E) yields a larger mixing width than the 2D solution (B) for all times. The 3D case with smaller A_{RMS} perturbations (F), however, has a very similar mixing width as the single mode case, suggesting that this increase in mixing width is strongly dependent on the magnitude of the small-scale perturbations.

The relative amount of molecular mixing can be computed through the mixedness ratio,

$$\Theta = W^{-1} \int_{-\infty}^{\infty} \overline{\xi(1 - \xi)} \, dz. \qquad (5)$$

Mixedness is a measure of the amount of mixing occurring between gasses, with 0 being unmixed and 1 being completely mixed. The mixedness for each case is shown in Fig. 4b. The mixedness decreases immediately following the passage of the shock wave due to the compression of the interface and early linear growth. The single mode only case (A) continues for the first 1 ms with little increase in mixedness. Once the small-scale perturbations become non-linear, they drive a rapid increase in mixedness for the cases with $A_{rms}/\eta = 0.03$ (cases B–F). The 3D cases (C–E) have a different behavior than in 2D and steadily increase in mixedness. The 3D case with a narrow depth (C) mirrors the behavior of the square domain case (D). At higher resolution (E) there is 10–20 % less mixing at early time, but the result converges to the lower resolution case (D) by the end of the simulation. The 3D case with smaller perturbations (F) follows the trend of the 2D single mode simulation until 0.75 ms, when it begins to have increased mixedness.

Conclusions

This study has shown that 3D effects are important in completely understanding the development of the RMI, even when the flow is dominated by 2D features. The simulation with 3D small-scale perturbations of $A_{RMS}/\eta = 0.003$ shows visual agreement with the experimental images. Spike height and growth rate is not significantly affected by smaller-scale perturbations, but the amount of mixing occurring is strongly dependent on small-scale features and is increased by 3D effects. Computing the solution using only a single mode perturbation shows that very little mixing occurs, while adding small-scale perturbations greatly increases the amount of mixing, yet that amount depends on the magnitude of the small-scale perturbations and on the dimensionality of the simulation. This implies that a

two-dimensional domain will not be able to accurately predict all aspects of the RMI since, at a minimum, it will not predict a proper measure of the mixing. These 3D effects can be captured with only a narrow depth in the 3rd dimension, which would save on computational resources.

References

1. Rayleigh, L.: Investigation of the character of the equilibrium of an incompressible heavy fluid of variable density. Proc. Lond. Math. Soc. **14** (1), 170–177 (1883)
2. Taylor, G.: The instability of liquid surfaces when accelerated in a direction perpendicular to their planes. I. Proc. R. Soc. Lond. **201** (1065), 192–196 (1950)
3. Richtmyer, R.D.: Taylor instability in shock acceleration of compressible fluids. Commun. Pure Appl. Math. **13** (2), 297–319 (1960)
4. Meshkov, E.E.: Instability of a shock wave accelerated interface between two gases. NASA Tech. Transl. **13**, 1–14 (1970)
5. Tennekes, H., Lumley, J.L.: A First Course in Turbulence. The MIT press, Cambridge (1972)
6. Smalyuk, V.A., et al.: Hydrodynamic instability growth and mix experiments at the National Ignition Facility Phys. Plasmas (1994-present), **21** (5), 056301 (2014)
7. Smalyuk, V.A., et al.: First measurements of hydrodynamic instability growth in indirectly driven implosions at ignition-relevant conditions on the National Ignition Facility. Phys. Rev. Lett. **112** (18), 185003 (2014)
8. Motl, B., Oakley, J., Ranjan, D., Weber, C., Anderson, M., Bonazza, R.: Experimental validation of a Richtmyer-Meshkov scaling law over large density ratio and shock strength ranges. Phys. Fluids **21** (12), 126102 (2009)
9. Cook, A.W.: Artificial fluid properties for large-eddy simulation of compressible turbulent mixing. Phys. Fluids **19** (5), 055103 (2007)
10. Cabot, W.H., Cook, A.W.: Reynolds number effects on Rayleigh–Taylor instability with possible implications for type ia supernovae. Nat. Phys. **2** (8), 562–568 (2006)
11. Weber, C.R., Cook, A.W., Bonazza, R.: Growth rate of a shocked mixing layer with known initial perturbations. J. Fluid Mech. **725**, 372–401 (2013)
12. Weber, C., Motl, B., Oakley, J., Anderson, M., Bonazza, R.: Richtmyer–Meshkov parameter study. Fusion Sci. Technol. **56** (1), 460–464 (2009)